THE JOURNAL OF PHYSICAL CHEMISTRY C

Article

pubs.acs.org/JPCC

Unraveling the Atomistic Sodiation Mechanism of Black Phosphorus for Sodium Ion Batteries by First-Principles Calculations

K. P. S. S. Hembram, Hyun Jung, Byung Chul Yeo, Sung Jin Pai, Seungchul Kim, Kwang-Ryeol Lee, and Sang Soo Han*

Computational Science Research Center, Korea Institute of Science and Technology (KIST), Hwarangno 14-gil 5, Seongbuk-gu, Seoul 136-791, Republic of Korea

Supporting Information

ABSTRACT: As opposed to the standard graphite anode used for lithium (Li) ion batteries (LIBs), a standard anode material for sodium (Na) ion batteries (NIBs) has not yet been reported. Black phosphorus is potentially very attractive as an anode material for NIBs, as it has a layered structure similar to graphite but a greater interlayer distance. In this work, we propose an atomistic mechanism for the sodiation of black phosphorus, based on first-principles calculations. The layered structure of black phosphorus is maintained up to the composition of $Na_{0.25}P$, with *one-dimensional* sodiation (an intercalation process) occurring in the interlayer spaces of the black phosphorus, resulting in sliding of the phosphorene layers because one Na atom tends to bind to four P atoms. At Na levels beyond $Na_{0.25}P$, the intercalation process changes to an alloying process. Sodiation exceeding the critical composition leads to breaking of P−P bonds and eventual formation of an amorphous phase from the layered Na_xP structure. After the P−P bonds in the layered Na_xP structure are broken, in a progress in which staggered P−P bonds are preferentially broken rather than planar P−P bonds, P_2 dumbbells are generated. As sodiation proceeds further, most of the P_2 dumbbells become isolated P atoms. Thus, in the amorphous Na_3P phase, only low-coordinate P components such as isolated atoms (primarily) and dumbbells are found. We expect that our comprehensive understanding of the sodiation mechanism in black phosphorus will provide helpful guidelines in designing new types of black phosphorus anodes to obtain better performing NIBs.

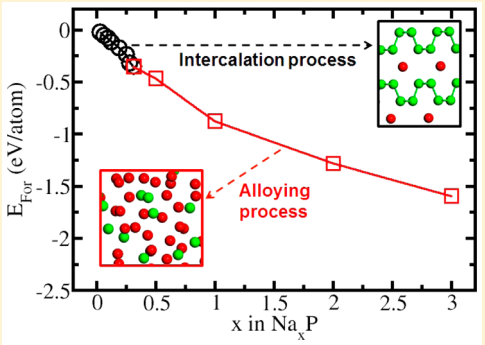

1. INTRODUCTION

In recent years, sodium (Na) ion batteries (NIBs) have drawn considerable attention as an alternative to lithium (Li) ion batteries (LIBs) because of the relatively high abundance of sodium and the similarities in the chemistries of sodium and lithium.[1−4] However, among several problems hindering the practical use of the NIBs, the absence of an appropriate anode material is one of the most serious.[5−7] In LIB, the graphite is regarded as the standard anode material; however, such a standard material is still unknown for NIB. While Li graphite intercalation compounds (Li-GICs) form a stage I structure in which every graphene layer is occupied by guest Li ions, Na-GICs do not form similar stage I structures.[8,9]

Recently, phosphorus, an element of the fifth group in the periodic table, has been studied as a potential anode material for LIBs and NIBs because of the natural abundance and environmental friendliness of phosphorus as well as a theoretical specific capacity predicted to be as high as 2596 mAh/g for Li_3P and Na_3P compounds.[10−12] Of the three phosphorus allotropes (red, white, and black), black phosphorus is most stable and has a layered structure similar to graphite consisting of phosphorene layers with AB stacking bound by van der Waals interactions.[13−15] The interlayer distance of black phosphorus is greater than that found in graphite (5.4 Å for black phosphorus vs 3.4 Å for graphite),[14−16] implying an easier intercalation of Na ions into the layers of black phosphorus than to the layers of graphite. Thus, black phosphorus can be considered as a potential anode material for the NIBs. Experimentally, black phosphorus shows a charge capacity (Na ion insertion) of 2035 mAh/g, although its reversible discharge capacity (Na ion removal) is decreased to 637 mAh/g. In addition, the Na charge/discharge capacities of black phosphorus are higher than those of amorphous red phosphorus (charge capacity: 897 mAh/g; discharge capacity: 15 mAh/g)[17] due to the higher bulk conductivity of black phosphorus.

To improve the battery performance of black phosphorus in NIBs, a thorough understanding of their sodiation mechanisms at the atomic scale is critically important. As mentioned, black phosphorus has many advantageous characteristics for the NIB anode applications; however, the study of the sodiation of black phosphorus is in its infancy, although density functional theory (DFT) works on the lithiation[18] and sodiation[19] mechanisms of phosphorene (the 2D counterpart of layered black phosphorus) were reported. Also, DFT studies on the comparative diffusion

Received: June 9, 2015
Published: June 13, 2015

DOI: 10.1021/acs.jpcc.5b05482
J. Phys. Chem. C 2015, 119, 15041−15046

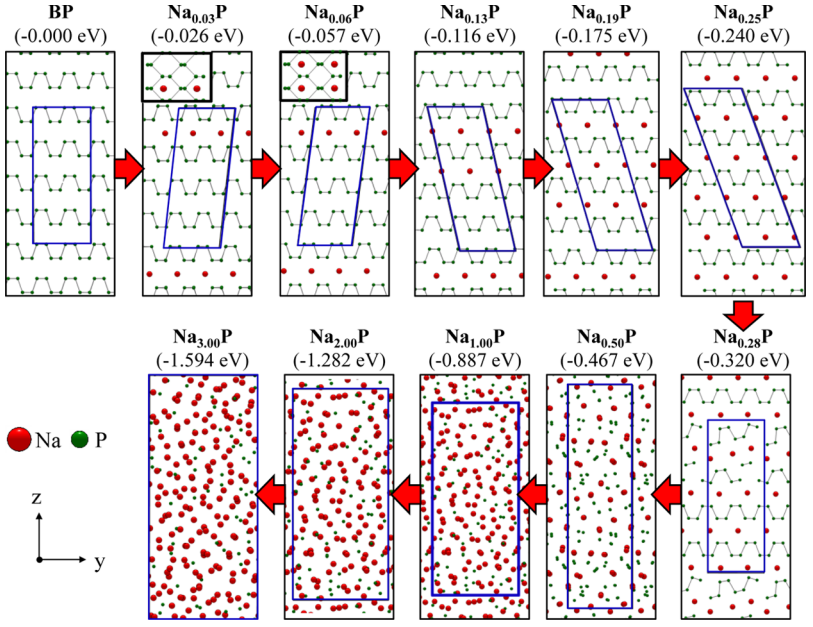

Figure 1. A sodiation mechanism of black phosphorus. Here, the numbers in parentheses indicate calculated formation energies of Na_xP structures. The blue solid lines indicate cell sizes of Na_xP including 64 P atoms used in our DFT calculations, and the black insets in $Na_{0.03}P$ and $Na_{0.06}P$ structures show top views of each structure to clarify positions of Na atoms in the structures.

of lithium and sodium in black phosphorus[20] and the sodium diffusion in crystalline Na_3P[21] were very recently reported. In the present work, we report a comprehensive DFT study on the sodiation mechanism of black phosphorus at the atomic level.

2. COMPUTATIONAL DETAILS

We performed periodic *ab initio* density functional theory (DFT) calculations as implemented in the Vienna *ab initio* simulation package (VASP).[22,23] The exchange-correlation energy is described by the generalized gradient approximation (GGA) proposed by Perdew, Burke, and Ernzerhof (PBE).[24] The electronic wave functions were expanded on a plane-wave basis set with a kinetic energy cutoff of 500 eV. The effects of core electrons were replaced by projector augmented wave (PAW) potentials.[25] To include the effect of van der Waals interactions, we adopted Grimme's DFT-D2 approach[26] implemented in the VASP software.

To investigate Na adsorption and diffusion, black phosphorus was modeled using a $2 \times 2 \times 2$ supercell with four phosphorene layers (total 64 P atoms). The Brillion zone was sampled using a $3 \times 2 \times 1$ Monkhorst–Pack grid.[27] The atomic structures of Na_xP were fully optimized without any symmetry constraint. For structural optimizations, the magnitudes of the forces on the atoms were minimized to be below the limit of 0.001 eV/Å. Our calculation provides lattice parameters of the black phosphorus crystal (a = 3.32 Å, b = 4.41 Å, and c = 10.49 Å) similar to experimental values (a = 3.34 Å, b = 4.49 Å, and c = 10.81 Å).[28]

To examine the Na diffusion pathways in black phosphorus, we also performed nudged elastic band (NEB) calculations.[29] For each pair of configurations with Na in equivalent binding sites, we sampled the corresponding pathway for diffusion with a NEB path consisting of five intermediate configurations. The NEB path was first constructed by linear interpolation of the atomic coordinates and then relaxed until the force on each atom was smaller in magnitude than 0.004 eV/Å.

3. RESULTS AND DISCUSSION

3.1. Sodiation Mechanism. In the present study, we focused on providing an understanding of the atomistic sodiation process in black phosphorus, an important phenomenon in the NIB anode. On the basis of DFT calculations for several Na_xP systems, we have elucidated the atomistic sodiation of black phosphorus, as shown in Figure 1. We calculated the formation energies of the Na_xP compounds with the following equation:

$$E_f(x) = E_{tot}(Na_xP) - E_{tot}(P) - xE_{tot}(Na) \quad (1)$$

In eq 1, $E_{tot}(Na_xP)$ is the total energy per Na_xP unit, $E_{tot}(Na)$ is the total energy per atom in the *bcc* Na crystal, and $E_{tot}(P)$ is the total energy per atom in the bulk black phosphorus.

We first investigated whether the initial two Na atoms intercalated into the black phosphorus preferred being in the same layer or in different layers in the formation of Na_2P_{64} ($Na_{0.03}P$) systems. According to Figure S1 of the Supporting Information, the arrangement wherein two Na atoms occupy the same layer in black phosphorus is thermodynamically preferred, despite the fact that the Na atoms in black phosphorus have positive atomic charges (Bader charge: +0.78e) that exert repulsive forces between one another. However, intercalation of the Na atoms into the same layer space leads to a minimum increase of the interlayer space and hence has the lowest energy cost.

Based on the formation energies for Na_4P_{64} ($Na_{0.06}P$) and Na_6P_{64} ($Na_{0.09}P$) (Figures S2 and S3), Na atoms are located at the same layer space up to θ = 25% coverage per phosphorene layer. Beyond this coverage, additional Na atoms fill different layers of black phosphorus, a trend that continues up to a composition of $Na_{0.25}P$, as shown in Figure 1. We also found that there is no P–P bond breaking in the black phosphorus at Na concentrations below $Na_{0.25}P$. Pristine black phosphorus has a planar P–P distance of 2.22 Å in the same corrugated half-layer and a staggered P–P distance of 2.26 Å in different corrugated half-layers with an interlayer distance of 5.40 Å. In

DOI: 10.1021/acs.jpcc.5b05482
J. Phys. Chem. C 2015, 119, 15041–15046

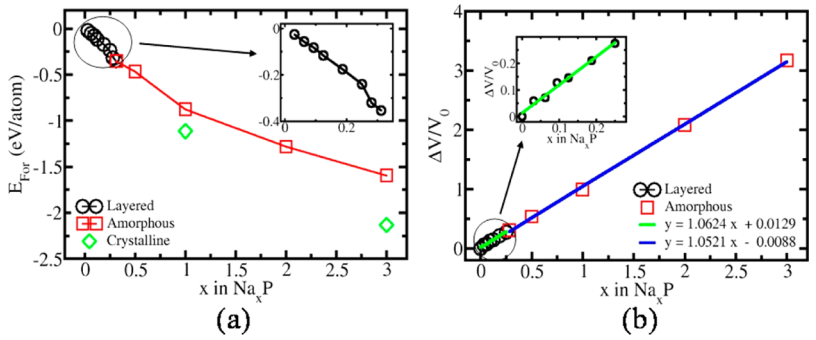

Figure 2. (a) Calculated formation energy and (b) volume expansion of Na_xP systems. Here, the inset in each figure corresponds to data for the layered black phosphorus region at the low Na concentrations. In (a), formation energies for crystalline Na_1P and Na_3P are also included for the comparison.

the $Na_{0.25}P$ structure, with an interlayer distance of 6.84 Å, the planar P−P distance is 2.23 Å and the staggered P−P distance is 2.29 Å, which are similar to the bond lengths in pristine black phosphorus. Sodiation of the black phosphorus does not significantly affect the chemical bonds between P atoms at Na levels below $Na_{0.25}P$ but instead simply increases the interlayer distance.

The sodiation of the layered spaces of black phosphorus induces changes in the layer stacking, as shown in Figure S4. In the layered structures of Na_xP, one Na atom tends to bind to four P atoms, with the Na−P bond formation (bond distance: 2.90 Å) leading to sliding of the phosphorene layers. We also calculated the energy required for this sliding in black phosphorus (Figure S5) and found that the energy required is marginal by 0.08 eV/atom, indicating the ease with which this sliding motion occurs.

However, when two more Na atoms are added into the $Na_{0.25}P$ structure, with a resultant $Na_{0.28}P$ composition, the process of P−P bond cleavage begins. Further sodiation eventually leads to the formation of an amorphous phase from the layered Na_xP structures. After P−P bond breakage, P_2 dumbbells are generated, as can be seen in the structure of $Na_{0.28}P$ (Figure 1). Further sodiation generates more of the P_2 dumbbells, as observed in the structure of $Na_{0.50}P$ (Figure 1). As the sodiation continues, most of the P_2 dumbbells become isolated P atoms. Thus, in the amorphous Na_3P phase, only low-coordinate P components, such as isolated atoms (primarily) and dumbbells, are found.

From the results thus far described, in Na concentrations above the critical composition of $Na_{0.25}P$, the sodiation mechanism of black phosphorus changes from a process of intercalation into the phosphorene layers to a process of alloying with P atoms. These mechanisms are clearly shown in Figure 1. In addition, according to the calculated atomic charges in the Na_xP structures (Figure S6), the atomic charges of Na in the layered Na_xP phase up to $x = 0.25$ show a constant value of $+0.78e$; however, the Na charge states in the amorphous phase decrease with increasing Na concentration and are distributed across a wide range due to increased interaction between Na atoms with increasing Na concentrations.

Figure 2a shows the calculated formation energies of the Na_xP systems. The formation energy gradually decreases up to the Na_3P composition, corresponding to a specific capacity of 2596 mAh/g. Comparisons with other NIB anode materials show that this specific capacity is higher than those for $Na_{0.76}Si$ (725 mAh/g),[30] $Na_{1.56}Ge$ (576 mAh/g),[30] $Na_{3.75}Sn$ (846 mAh/g),[31] $Na_{3.75}Pb$ (854 mAh/g),[31] and Na_3Sb (660 mAh/g).[32] After full sodiation (Na_3P), black phosphorus shows a volume expansion of 317% (Figure 2b) similar to the 293% expansion known for Na_3Sb.[32] In general, the volume expansion of black phosphorus increases linearly with Na concentration, despite the fact that the sodiation mechanism changes from an intercalation process to an alloying process above the critical composition ($Na_{0.25}P$). In other words, the slope of V/V_0 versus x in Na_xP is 1.06 for layered Na_xP and 1.05 for amorphous Na_xP.

3.2. Investigating P−P Bond Breaking Mechanism. To elucidate the formation of amorphous Na_xP structures at the atomic level, we scrutinized the breaking of P−P bonds induced by sodiation. Figure 3a shows the electronic charge density distribution on a (010) plane of $Na_{0.28}P$ at the point when P−P bond breaking begins. Most of the electronic charge is accumulated around P atoms, rather than Na atoms, indicating

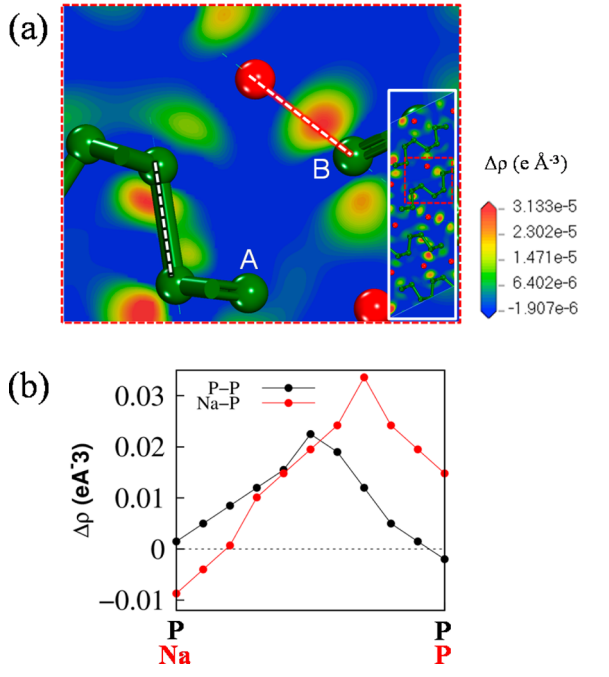

Figure 3. (a) Valence electron charge density distribution on a (010) plane in the $Na_{0.28}P$. Here green and red atoms are P and Na atoms, respectively. (b) The charge density difference distribution along a P−P bond represented by a black dashed line in (a) and the Na−P bond represented by a red dashed line in (a).

DOI: 10.1021/acs.jpcc.5b05482
J. Phys. Chem. C 2015, 119, 15041−15046

partial charge transfer from Na to P. A close inspection of the charge density plot shows that the bond between P atoms A and B is indeed broken. The dangling P atoms, created upon P−P bond breakage, can be saturated by Na atoms, leading to Na−P bonds with predominantly ionic bond character. For a clearer picture, we also plotted the charge density difference distribution (Figure 3b) along a Na−P bond (red line in Figure 3a). The charge density difference $\Delta\rho$ is defined as follows:

$$\Delta\rho = \rho_{Na_{0.28}P} - \rho_P - \rho_{Na} \quad (2)$$

In eq 2, $\rho_{Na_{0.28}P}$, ρ_P, and ρ_{Na} are the electron densities of the $Na_{0.28}P$ system, a phosphorus structure consisting of only P atoms in the same positions as in the $Na_{0.28}P$ structure, and the contribution from the individual Na atoms at the positions they occupy in the $Na_{0.28}P$ system, respectively. This plot clearly shows that the charge density difference around the P atom is positive (charge accumulation), while it is negative around the Na atom (charge depletion), indicating charge transfer from Na to P resulting from the electronegativity difference of the two atoms. In contrast to the Na−P bond, we see a symmetric electron charge accumulation between pairs of P nearest neighbors (black lines in Figure 3b).

As already mentioned, black phosphorus has a corrugated structure, providing two different P−P bonds called *planar* P−P and *staggered* P−P. Interestingly, sodiation leads to preferential breaking of the staggered P−P bonds rather than the planar ones, as seen in the $Na_{0.28}P$ structure (Figure 1). To clarify the reason for this phenomenon, we calculated the energy changes of the Na_xP structures as a function of the change in the bond distance for each P−P bond. In calculating the energy change, we optimized the Na_xP structure along with a cell optimization, in which the positions of two P−P bond atoms were fixed at a given bond distance while the other P and Na atoms were allowed to relax.

Figure 4 shows the energy profile as a function of P−P bond elongation. The slopes of planar bonds are steeper than those

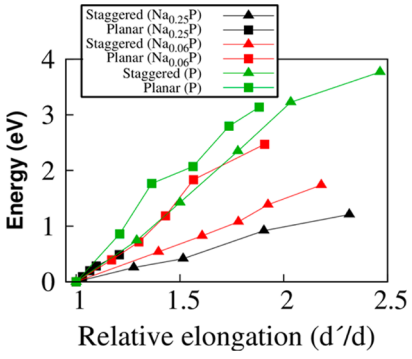

Figure 4. Energy profiles with elongation (d'/d) of planar (square) and staggered (triangle) P−P bonds in pristine black phosphorus (P), $Na_{0.06}P$, and $Na_{0.25}P$, where d is an optimized P−P bond distance and d' is an elongated bond distance.

of staggered ones, clearly indicating that more energy is required to break planar P−P bonds than staggered P−P bonds. The intercalation of Na atoms into black phosphorus leads to a significant increase in the interlayer distance along the c direction rather than along the a or b direction. Thus, geometry changes of the P atoms in the Na_xP (e.g., $Na_{0.28}P$) structure, induced by additional sodiation in the layered $Na_{0.25}P$, are more facile (less steric hindrance) along the c direction than along the a or b direction, explaining the relative ease with which staggered P−P bonds are broken. Moreover, sodiation in the layered Na_xP structures leads to sliding of the phosphorene layers, as shown in Figure S4. During the sliding motion, the planar P−P bonds are left essentially unaffected, as they occupy the same plane as the direction of the sliding; however, the staggered P−P bonds accumulate lateral stress (Figure S7), resulting in easier breakage of the staggered P−P bonds than the planar P−P bonds.

Figure 4 also shows that the slopes of both the planar and staggered bonds decrease with degree of sodiation. This indicates that it is easier to break P−P bonds in sodiated Na_xP structures than in pristine black phosphorus, supporting the hypothesis that increased sodiation leads to amorphous Na_xP.

3.3. Diffusion of a Na Atom in Black Phosphorus.

Layered sodiation can be more thoroughly envisaged by studying the diffusion behavior of a Na atom in black phosphorus. We performed NEB calculations to investigate the diffusion pathways of a single Na atom. Figure 5 shows the

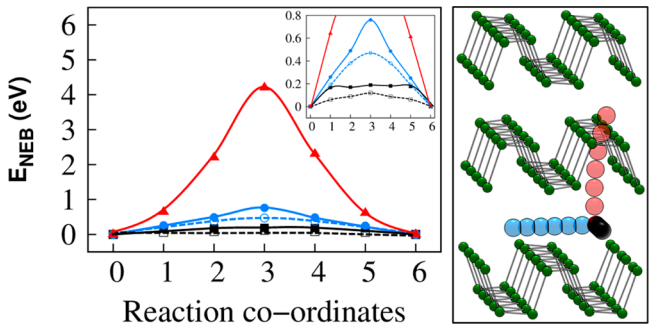

Figure 5. NEB calculations on diffusion barriers of a Na atom in black phosphorus (solid symbols) and on a phosphorene single layer (open symbols). The color codes correspond to the diffusion pathways in the right figure.

NEB barriers to Na diffusion along three possible paths in black phosphorus, of which two correspond to behaviors along the phosphorene layer and the other corresponds to interpenetration through a phosphorus hexagon ring of the phosphorene layer. For the diffusion behaviors along the phosphorene layer, the Na atom hops along the same channel direction (black route in Figure 5) or hops to an adjacent channel along the corrugated path (blue route in Figure 5). The former route has a diffusion barrier of 0.18 eV, while the latter has a 0.76 eV barrier, indicating that the diffusion of Na atoms along the one-dimensional pore channels in black phosphorus (the former route) is an easy process. In contrast, the diffusion barrier for interlayer Na diffusion (red route in Figure 5) is very high by 4.2 eV, much higher than the energy associated with diffusion along the phosphorene layer. It is very difficult for a Na atom to penetrate the hexagonal rings of the phosphorene layer. Instead, Na atoms show one-dimensional diffusion paths along the pore channels of black phosphorus, similar to diffusion behavior along the pores of nanotube materials.

4. CONCLUSION

In conclusion, we have proposed a sodiation mechanism of black phosphorus at the atomic level, based on first-principles calculations. The sodiation of black phosphorus occurs via layered intercalation up to a composition of $Na_{0.25}P$, beyond

DOI: 10.1021/acs.jpcc.5b05482
J. Phys. Chem. C 2015, 119, 15041−15046

which further sodiation leads to P−P bond cleavage and eventual formation of amorphous Na_xP, concomitant with large volume expansion. It is proposed that improved anode performance of black phosphorus in NIBs relies on the maintenance of the layered structures, as these layers provide better kinetic (easier diffusion of Na atoms) and cyclic (no phase transition from the layered structure to the amorphous one) properties, although such layered structures might have a disadvantage that electrolyte molecules would intercalate into the layer spaces and then lead to exfoliation of the layered structures. Black phosphorus−graphite composites, similar to those described in a previous report (ref 33), are one option for improving the stability of the layered structure of black phosphorus during sodiation. In such composites, formation of stable phosphorus−carbon bonds would enhance the stability of the layered structure of black phosphorus. Additionally, pillared black phosphorus could be another option. The pillar may not only improve the stability of the layered structure of black phosphorus but also increase the interlayer distance of black phosphorus, providing easy diffusion channels for Na atoms. In these endeavors, the selection or design of an appropriate pillar capable of forming strong chemical bonds with phosphorene layers would be very important and will be investigated in our future work.

■ ASSOCIATED CONTENT

Supporting Information

Formation energies and atomic structures of several Na_xP (x = 0.03, 0.06, and 0.09), energy changes of black phosphorus with sliding movement of a phosphorene layer, and Bader charge populations of Na in Na_xP. The Supporting Information is available free of charge on the ACS Publications website at DOI: 10.1021/acs.jpcc.5b05482.

■ AUTHOR INFORMATION

Corresponding Author

*E-mail sangsoo@kist.re.kr; Tel +82 2 958 5441; Fax +82 2 958 5451 (S.S.H.).

Notes

The authors declare no competing financial interest.

■ ACKNOWLEDGMENTS

We acknowledge the financial support of the Korea Institute of Science and Technology (Grants 2E25372 and 2E25630) and the Industrial Strategic Technology Development Program (Grant 10041589) funded by the Ministry of Trade, Industry, and Energy (MOTIE) of Korea.

■ REFERENCES

(1) Ong, S. P.; Chevrier, V. L.; Hautier, G.; Jain, A.; Moore, C.; Kim, S.; Ma, X.; Ceder, G. Voltage, stability and diffusion barrier differences between sodium-ion and lithium-ion intercalation materials. *Energy Environ. Sci.* **2011**, *4*, 3680−3688.

(2) Kim, S.-W.; Seo, D.-H.; Ma, X.; Ceder, G.; Kang, K. Electrode materials for rechargeable sodium-ion batteries: Potential alternatives to current lithium-ion batteries. *Adv. Energy Mater.* **2012**, *2*, 710−721.

(3) Palomares, V.; Serras, P.; Villaluenga, I.; Hueso, K. B.; Gonzalez, J. C.; Rojo, T. Na-ion batteries, recent advances and present challenges to become low cost energy storage systems. *Energy Environ. Sci.* **2012**, *5*, 5884−5901.

(4) Hong, S. Y.; Kim, Y.; Park, Y.; Choi, A.; Choi, N.-S.; Lee, K. T. Charge carriers in rechargeable batteries: Na ions vs. Li ions. *Energy Environ. Sci.* **2013**, *6*, 2067−2081.

(5) Chevrier, V. L.; Ceder, G. Challenges for Na-ion negative electrodes. *J. Electrochem. Soc.* **2011**, *158* (9), A1011−A1014.

(6) Mortazavi, M.; Deng, J.; Shenoy, V. B.; Medhekar, N. V. Elastic softening of alloy negative electrodes for Na-ion batteries. *J. Power Sources* **2013**, *225*, 207−214.

(7) Slater, M. D.; Kim, D.; Lee, E.; Johnson, C. S. Sodium-ion batteries. *Adv. Funct. Mater.* **2013**, *23*, 947−958.

(8) Persson, K.; Sethuraman, V. A.; Hardwick, L. J.; Hinuma, Y.; Meng, Y. S.; van der Ven, A.; Srinivasan, V.; Kostecki, R.; Ceder, G. Lithium diffusion in graphitic carbon. *J. Phys. Chem. Lett.* **2010**, *1*, 1176−1180.

(9) Okamoto, Y. Density functional theory calculations of alkali metal (Li, Na, and K) graphite intercalation compounds. *J. Phys. Chem. C* **2014**, *118*, 16−19.

(10) Sun, L.-Q.; Li, M.-J.; Sun, K.; Yu, S.-H.; Wang, R.-S.; Xie, H.-M. Electrochemical activity of black phosphorus as an anode material for lithium-ion batteries. *J. Phys. Chem. C* **2012**, *116*, 14772−14779.

(11) Wang, L.; He, X.; Li, J.; Sun, W.; Gao, J.; Guo, J.; Jiang, C. Nano-structured phosphorus composite as high-capacity anode materials for lithium batteries. *Angew. Chem., Int. Ed.* **2012**, *51*, 9034−9037.

(12) Kim, Y.; Park, Y.; Choi, A.; Choi, N.-S.; Kim, J.; Lee, J.; Ryu, J. H.; Oh, S. M.; Lee, K. T. An amorphous red phosphorus/carbon composite as a promising anode material for sodium ion batteries. *Adv. Mater.* **2013**, *25*, 3045−3049.

(13) Bridgman, P. W. Two new modifications of phosphorus. *J. Am. Chem. Soc.* **1914**, *36*, 1344−1363.

(14) Hultgren, R.; Gingrich, N. S.; Warren, B. E. The atomic distribution in red and black phosphorus and the crystal structure of black phosphorus. *J. Chem. Phys.* **1935**, *3*, 351−355.

(15) Du, Y.; Ouyang, C.; Shi, S.; Lei, M. Ab initio studies on atomic and electronic structures of black phosphorus. *J. Appl. Phys.* **2010**, *107*, 093718−4.

(16) Bacon, G. E. The interlayer spacing of graphite. *Acta Crystallogr.* **1951**, *4*, 558−561.

(17) Qian, J.; Wu, X.; Cao, Y.; Ai, X.; Yang, H. High Capacity and rate capability of amorphous phosphorus for sodium ion batteries. *Angew. Chem., Int. Ed.* **2013**, *52*, 4633−4636.

(18) Zhao, S.; Kang, W.; Xue, J. The potential application of phosphorene as an anode material in Li-ion batteries. *J. Mater. Chem. A* **2014**, *2*, 19046−19052.

(19) Kulish, V. V.; Malyi, O. I.; Persson, C.; Wu, P. Phosphorene as an anode material for Na-ion batteries: A first-principles study. *Phys. Chem. Chem. Phys.* **2015**, *17*, 13921−13928.

(20) Yu, X-f.; Ushiyama, H.; Yamashita, K. Comparative study of sodium and lithium intercalation and diffusion mechanism in black phosphorus from first-principles simulation. *Chem. Lett.* **2014**, *43*, 1940−1942.

(21) Yu, X-f.; Giorgi, G.; Ushiyama, H.; Yamashita, K. First-principles study of fast Na diffusion in Na_3P. *Chem. Phys. Lett.* **2014**, *612*, 129−133.

(22) Kresse, G.; Furthmüller, J. Efficient iterative schemes for *ab-initio* total-energy calculations using a plane-wave basis set. *Phys. Rev. B* **1996**, *54*, 11169−11186.

(23) Kresse, G.; Furthmüller, J. Efficiency of ab-initio total energy calculations for metals and semiconductors using a plane-wave basis set. *Comput. Mater. Sci.* **1996**, *6*, 15−50.

(24) Perdew, J. P.; Burke, K.; Ernzerhof, M. Generalized gradient approximation made simple. *Phys. Rev. Lett.* **1996**, *77*, 3865−3868.

(25) Blöchl, P. E. Projector augmented-wave method. *Phys. Rev. B* **1994**, *50*, 17953−17979.

(26) Grimme, S. Semiempirical GGA-type density functional constructed with a long range dispersion correction. *J. Comput. Chem.* **2006**, *27*, 1787−1799.

(27) Monkhorst, H. J.; Pack, J. D. Special points for Brillonin-zone integrations. *Phys. Rev. B* **1976**, *13*, 5188−5192.

(28) Brown, A.; Rundqvist, S. Refinement of the crystal structure of black phosphorus. *Acta Crystallogr.* **1965**, *19*, 684−685.

DOI: 10.1021/acs.jpcc.5b05482
J. Phys. Chem. C 2015, 119, 15041−15046

(29) Henkelman, G.; Uberuaga, B. P.; Jónsson, H. A climbing image nudged elastic band method for finding saddle points and minimum energy paths. *J. Chem. Phys.* **2000**, *113*, 9901−9904.
(30) Jung, S. C.; Jung, D. S.; Jung, W. C.; Han, Y.-K. Atom-level understanding of the sodiation process in silicon anode material. *J. Phys. Chem. Lett.* **2014**, *5*, 1283−1288.
(31) Komaba, S.; Matsuura, Y.; Ishikawa, T.; Yabuuchi, N.; Murata, W.; Kuze, S. Redox reaction of Sn-polyacrylate electrodes in aprotic Na cell. *Electrochem. Commun.* **2012**, *21*, 65−68.
(32) Baggetto, L.; Ganesh, P.; Sun, C.-N.; Meisner, R. A.; Zawodzinski, T. A.; Veith, G. M. Intrinsic thermodynamic and kinetic properties of Sb electrodes for Li-ion and Na-ion batteries: experiment and theory. *J. Mater. Chem. A* **2013**, *1*, 7985−7994.
(33) Sun, J.; Zheng, G.; Lee, H.-W.; Liu, N.; Wang, H.; Yao, H.; Yang, W.; Cui, Y. Formation of stable phosphorus-carbon bond for enhanced performance in black phosphorus nanoparticle-graphite composite battery anodes. *Nano Lett.* **2014**, *14*, 4573−4580.

DOI: 10.1021/acs.jpcc.5b05482
J. Phys. Chem. C 2015, 119, 15041−15046